

● *Brief Communication*

**QUANTIFYING REGIONAL HYPOXIA IN HUMAN TUMORS WITH
POSITRON EMISSION TOMOGRAPHY OF [¹⁸F]FLUOROMISONIDAZOLE:
A PRETHERAPY STUDY OF 37 PATIENTS**

JANET S. RASEY, PH.D.,* WUI-JIN KOH, M.D.,* MARGARET L. EVANS, M.A.,*
LANELL M. PETERSON, B.A.,* THOMAS K. LEWELLEN, PH.D.,[†]
MICHAEL M. GRAHAM, PH.D., M.D.*[†] AND KENNETH A. KROHN, PH.D.,*[†]

Departments of Radiation Oncology and Radiology,[†] University of Washington, Seattle, WA

Purpose: To assess pretreatment hypoxia in a variety of tumors using positron emission tomography (PET) after injection of the hypoxia-binding radiopharmaceutical [¹⁸F]fluoromisonidazole ([¹⁸F]FMISO).

Methods and Materials: Tumor fractional hypoxic volume (FHV) was determined in 21 nonsmall cell lung cancer patients, 7 head and neck cancer patients, 4 prostate cancer patients, and 5 patients with other malignancies by quantitative PET imaging after injection of [¹⁸F]FMISO (0.1 mCi/kg). The FHV was defined as the proportion of pixels in the imaged tumor volume with a tissue:blood [¹⁸F] activity ratio ≥ 1.4 at 120–160 min postinjection. A FHV > 0 was taken as evidence for tumor hypoxia.

Results: Hypoxia was observed in 36 of 37 tumors studied with FMISO PET imaging; FHVs ranged from 0 to 94.7%. In nonsmall cell lung cancers ($n = 21$), the median FHV was 47.6% and the range, 1.3 to 94.7%. There was no correlation between tumor size and FHV. In the seven head and neck carcinomas, the median FHV was 8.8%, with a range from 0.2 to 18.9%. In the group of four prostate cancers, the median and range were 18.2% and 0 to 93.9%, while in a group of five tumors of different types the median FHV was 55.2% (range: 21.4 to 85.8%).

Conclusions: Hypoxia was present in 97% of the tumors studied and the extent of hypoxia varied markedly between tumors in the same site or of the same histology. Hypoxia also was distributed heterogeneously between regions within a single tumor. These results are consistent with O₂ electrode measures with other types of human tumors. The intra- and intertumor variability indicate the importance of making oxygenation measures in individual tumors and the necessity to sample as much of the tumor volume as possible. Copyright © 1996 Elsevier Science Inc.

Hypoxia, Imaging, Positron emission tomography, [¹⁸F]fluoromisonidazole.

INTRODUCTION

Detecting and quantifying oxygen levels in human tumors has potentially high impact on predicting outcome of tumor treatment with radiation and possibly some chemotherapeutic agents. Hypoxia has long been implicated as a negative prognosticator for local control after radiation therapy (6). Hypoxia makes some cells more resistant to selected anticancer drugs, while other chemotherapeutic agents are more effective against oxygen-deprived cells (39–40, 42). Cells that have been reoxygenated after several hours of hypoxia may also be more resistant to chemotherapy (20, 27, 41). Quantifying tumor hypoxia also may further our understanding of malignant progression, which may be enhanced by hypoxia, or hypoxia followed by reoxygenation (1, 14, 46–47). Oxygen deprivation may enhance cellular changes leading to tumor progression,

such as increased vascularity stimulated by vascular endothelial growth factor (VEGF), (15), gene amplification that can lead to drug resistance (37, 38), and selection for cells with mutant p53 (10).

A renewed interest in measuring human tumor hypoxia followed the clinical availability of the Eppendorf pO₂ histogram. This instrument measures tissue pO₂ with polarographic electrodes and allows large numbers of measurements to be made in each tumor, more easily and with fewer artifacts than with other electrodes (19). Pretreatment pO₂ measured with the Eppendorf electrodes appears to predict outcome of radiotherapy in cervical cancer (16, 18). Earlier studies with less sophisticated O₂ electrodes, although allowing only a small number of measures per patient, also showed a strong correlation between pretherapy oxygen measures and outcome of radiation

Reprint requests to: Janet S. Rasey, Ph.D., Department of Radiation Oncology, University of Washington, Box 356069, Seattle, WA 98195-6069.

Acknowledgements—Source of Support: NIH/NCI Grant #PO1 CA42045.

Accepted for publication 5 June 1996.

treatment in cervical cancer (23) and in metastatic neck nodes in head and neck cancer (9).

The recent studies with electrodes have again pointed out the difficulties of this technically demanding and invasive technique. Investigators ideally need a variety of methods to measure regional tumor oxygenation. Noninvasive imaging with radiolabeled nitroimidazoles offers advantages over more invasive studies that require insertion of electrodes or acquisition of a biopsy, as for the comet assay (30) or cryospectrophotometry (7). In addition, the whole tumor, or a significant portion of it, can be imaged. Single photon emission computed tomography (SPECT) imaging of [¹²³I]iodoazomycin arabinoside (IAZA) (13, 31), and PET imaging of [¹⁸F]fluoromisonidazole (FMISO) (21–22, 43) have been developed to meet the need for noninvasive hypoxia imaging.

Our initial report of eight patients imaged with [¹⁸F]FMISO (22) described our protocols and established PET imaging as a contender for noninvasive monitoring of hypoxia. In this article we describe a refined and more accurate pixel-by-pixel analysis and report the quantification of pretreatment hypoxia with [¹⁸F]FMISO in 37 patients with tumors arising from various sites and of varying histologies. Our results suggest that human tumor hypoxia is widely prevalent and highly variable between different tumors of the same histology and also between regions within the same tumor.

METHODS AND MATERIALS

[¹⁸F]Fluoromisonidazole was synthesized from anhydrous [¹⁸F] fluoride via its incorporation into epifluorohydrin and subsequent coupling to 2-nitroimidazole, as described previously (12, 22). Specific activity, decay corrected to the end of ¹⁸F production, was 1.5–2.2 × 10¹³ Bq/mmol. An investigational new drug (IND) approval covering the use of [¹⁸F]FMISO was obtained from the Food and Drug Administration.

The tomograph (UW TOFPET) is a modified Scanditronix SP-3000 time-of-flight machine with four rings of BaF₂ detectors (320 crystals/ring) and has been described in more detail (25, 26). The tomograph was upgraded to a four-ring system in 1990, allowing collection of seven imaging planes; typically, four consecutive planes (14 mm thick) were imaged in a study. The tomograph utilized list mode data collection with timing markers that allowed selection of time binning or gating criteria during image reconstruction. The limiting resolution of the system was 5.5 mm transaxially and 11 mm in the axial direction. All images were reconstructed using a 12 mm filter.

Forty-two (42) tumor-bearing patients entered protocols to quantify human tumor hypoxia with the UW TOFPET. Eligible patients were those with tumors ≥ 2 cm in diameter who were seen at the University of Washing-

ton Cancer Center for radiotherapy of primary or recurrent cancers. Tumors at any site were eligible. All patients were scanned prior to or within the first week of their initiation of fractionated radiotherapy. Approval for the study protocol was obtained from the University of Washington human subjects review committee and the radiation safety committee, and all patients gave informed consent. Three imaging protocols, differing in degree of complexity, were employed for these studies (Table 1). While the continuous protocol gave data amenable to mathematical modeling to obtain radiobiologic hypoxic fraction (3), the simpler intermittent and brief protocols generated sufficient and equivalent data for calculation of the fractional hypoxic volumes (FHVs), defined and reported below and were more acceptable to the patients.

The results of 37 pretreatment imaging studies are reported here. Five of the initially selected 42 patients were eliminated for the following reasons: 1 patient received less than one-half of the usual dose of FMISO; his scans were not analyzed because of low count rate and poor image quality. One patient was initially imaged for 15 min in the intermittent protocol (Table 1) but failed to return for the second imaging session at 2 h postinjection. In three cases, the calibration factor comparing the gamma well counter, used for the blood samples, to the dose calibrator fell outside the acceptable range. This apparently was due to dilution errors in the calibration jug solution and meant that the conversion of the PET data to μCi/ml, for comparison to blood data in μCi/ml, could not be made. Of the 37 remaining patients, 21 had nonsmall cell lung cancer, 7 had head and neck tumors, 4 had prostate tumors, and the remaining 5 patients included 1 case each of cervical, rectal, metastatic breast, thyroid, and metastatic renal cell carcinoma.

Computed tomography (CT) scans were obtained for all patients to aid in planning their radiation treatment. These scans also were analyzed to localize the tumor for PET imaging, assess its size, and look for areas of reduced contrast enhancement suggestive of necrosis. After reconstruction of images, the CT scans guided us in drawing regions of interest (ROIs) for analysis of each of the PET imaging planes containing tumor. In 12 of the patients with nonsmall cell lung cancers, the extent of tumor in each CT plane was carefully measured and the tumor volume in cc calculated to allow correlation of tumor size with FHV.

The seven patients with head and neck tumors were placed in a customized foam mold to stabilize their heads and make them more comfortable during imaging. A 16 French Foley catheter was placed in the patients with prostate or cervical cancers during imaging to drain urine and thereby reduce radiation activity in the bladder, increase contrast between tumor and background, and reduce image reconstruction artifacts.

Patient positioning, described in Koh (22), took advantage of the pretherapy CT scan to determine tumor size and location, and gridded radiographs were obtained at

Table 1. Protocols used for patient imaging*

Type of protocol	No. of patients	Tomograph sequence, blood sampling
Continuous (Cont)	4	(1) 40 min acquisition of uptake in tumor (2) 15 min acquisition of normal tissue uptake data (3) 40 min acquisition of uptake in tumor (60–100 min postinjection) (4) 15 min acquisition of normal tissue uptake data (5) 40 min acquisition of uptake in tumor (120–160 min postinjection) (6) Optional 15 min acquisition of normal tissue uptake data (7) Frequent, timed arterial or venous blood throughout
Intermittent (Int)	26	(1) 15 min acquisition of uptake in tumor (2) Patient released from PET suite for approximately 90 min (3) 'Late' 40 min acquisition of uptake in tumor (120–160 min postinjection) (4) Timed venous blood samples at 0–15 min and 120–160 min postinjection
Brief	7	(1) 'Late' 40 min acquisition of uptake in tumor (120–160 min postinjection) (2) Timed venous blood samples at 120–160 min postinjection

PET = Positron emission tomography.

FMISO = Fluoromisonidazole.

* All imaging protocols were preceded by an attenuation scan obtained as described in Methods and Materials. The patient then received an i.v. injection of [¹⁸F]FMISO (0.1 mCi/kg) over a 2-min period, except in two of four of the early continuous protocols where the FMISO was injected more slowly, taking up to 8 min. Imaging began 1 min before injection in the intermittent and continuous protocols.

the tomograph, allowing PET imaging planes to be aligned with previously selected transverse CT slices. The patient's position in the tomograph was confirmed by tomograph laser beams, aligned with marks on the patient's body.

A PET attenuation scan with a rotating Ge-68 rod source was obtained prior to imaging. Two venous lines, one in each arm, were established, one for injecting [¹⁸F]FMISO and the other for blood sampling. In three early studies, a radial arterial line rather than a venous line was established to take frequent arterial samples with an automatic blood sampler (11).

Fluoromisonidazole (0.1 mCi/kg body weight, 3.7 MBq/kg, 0.1 nmol/kg) was injected intravenously over 2 min, except for injection times lasting up to 8 min in two of the early continuous protocols (Table 1). The times of data acquisition varied with the protocol (Table 1); however, for the analysis presented here, data acquired between 120 and 160 min postinjection were used to determine tumor FHV.

Blood samples were withdrawn periodically during the imaging period from 120 to 160 min postinjection as outlined in Table 1. In early studies plasma was obtained by centrifugation, but after finding that FMISO distributed equally between plasma and red cells, whole blood samples were used. Samples were counted in a Cobra multi-channel gamma well counter.¹

A 6 cm diameter calibration vial containing 500 ml [¹⁸F] solution (4% of the injected [¹⁸F]FMISO activity) was placed in the field of view, typically below the patient couch, and was imaged for 1 min prior to injection and during the acquisition of patient data. In addition to being imaged, samples from this vial were counted in the same gamma well counter as were the blood samples. Imaging and gamma well counting of the calibration jug solution allowed us to convert PET data in counts/pixel-s to cpm/ml and μ Ci/ml, correct for decay, cross calibrate between the dose calibrator and the gamma counter, and correct for tomograph counting efficiency. Blood activity also was expressed as μ Ci/ml.

The list-mode data acquisition, reconstruction of attenuation-corrected time-binned images, and transfer of data to Macintosh work stations for image analysis have been described previously (22). With the aid of the CT and attenuation scans, ROIs were drawn to encompass the entire tumor, several regions of normal tissue (typically muscle, lung, and brain), a background area, and the [¹⁸F] calibration vial and background immediately around the vial. All imaging planes containing tumor were analyzed. Data were initially available as counts/pixel-s but were subsequently converted to μ Ci/ml of tissue for each pixel in the selected ROI, as described above. This allowed a pixel-by-pixel calculation of tumor: blood or tissue: blood activity ratios summed for all image planes. The proportion of

¹Packard Corp., Meriden, CT.

pixels in the imaged tumor volume with a tissue:blood ratio ≥ 1.4 , representative of significant hypoxia relative to normal tissue, was calculated to determine a fractional hypoxic volume. The presentation of PET images of tumors with a bimodal color scale to demonstrate the proportion of the tumor with a tissue:blood ratio ≥ 1.4 , has been described previously (22).

We selected a tissue:blood FMISO retention ratio ≥ 1.4 at 2 or more h after FMISO injection as indicative of substantial hypoxia. This was based on tissue:blood ratios for 1342 samples from four normal tissues (lung, brain, heart, and skeletal muscle) in four animal species (rat, mouse, dog, and gerbil) (22). Ninety percent of the presumed normoxic tissues had a tissue:blood ratio ≤ 1.31 , and, thus, a ratio of 1.4 was taken as a conservative estimate of FMISO concentration associated with hypoxia. Tissue:blood ratios were obtained from muscle in 28 patients (49 planes of data) and from brain in 9 patients (17 planes of data), for comparison to the animal tissue data to determine if the cutoff value of 1.4, initially derived from animal tissues, needed to be changed.

Certain factors contribute to uncertainty of FHV calculations. The fractional variation in counting data is approximately equal to five divided by the square root of the counts. The coefficient of five arises from scaling of the data that occurs during attenuation correction. Thus in patients with low counts, this might lead to some pixels with an artifactual tissue:blood ratio > 1.4 and a suggestion of hypoxia where in fact there was none. For this reason, the standard dose of [^{18}F]FMISO was 0.1 milliCurie/kg body weight, and one patient was rejected from analysis because of low counts, as described above. FMISO is excreted principally through the kidneys, raising the possibility that differences in clearance rate could influence our imaging results. However, imaging data were collected from 120 to 160 min postinjection, in part to avoid early differences in clearance of tracer that might depend on variation in kidney function.

RESULTS

We first examined normal tissue:blood FMISO uptake ratios in patients to assess whether the cutoff value of 1.4, defined as indicative of hypoxia in animal tissues, was still appropriate for humans. Imaging of muscle and normal brain for dosimetry purposes allowed us to establish normal tissue FMISO retention patterns, at 120 to 160 min postinjection, in two of the same tissues that had been evaluated in animals. The frequency distributions of human muscle:blood ratios (Fig. 1A) and brain:blood ratios (Fig. 1B) are markedly similar to that for animal tissues. The median muscle:blood ratio was 0.98, and 87% of the values are below 1.4. The fraction of values below 1.4 is very similar to that reported from animal tissues (22). For brain, where many fewer patients were imaged, the median ratio was 1.21, and 83% of the measurements fall below 1.4. We have, thus, retained 1.4 as the cutoff ratio

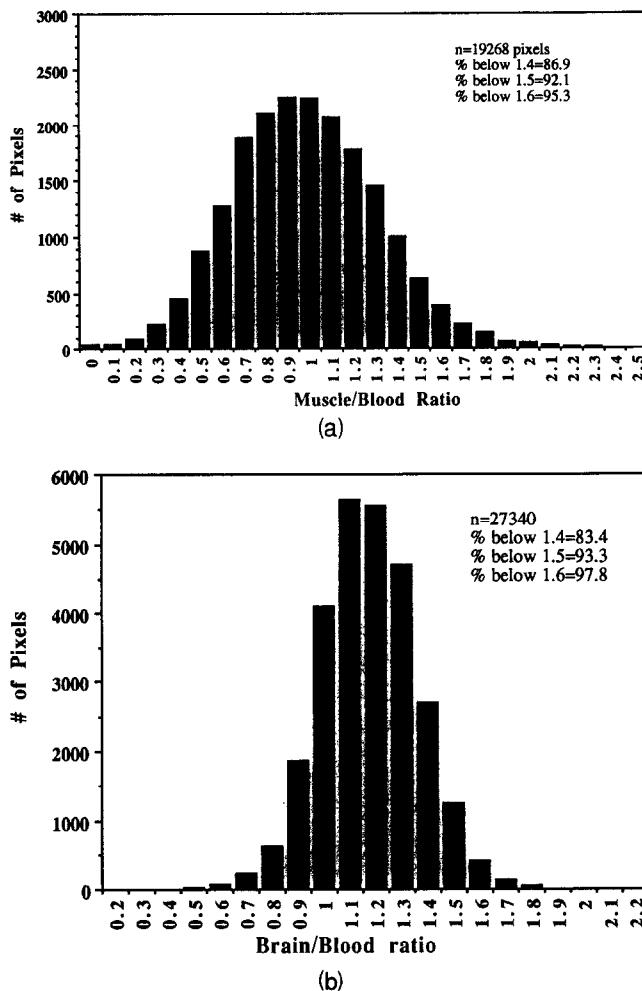


Fig. 1. (a) Histogram of human muscle:blood ratios for [^{18}F]fluoromisonidazole. (b) Histogram of human brain:blood ratios for [^{18}F]fluoromisonidazole.

indicative with hypoxic tissue to be consistent with our other published reports (21, 22).

Our results present a thorough analysis of regional hypoxia throughout the imaged tumor volume in 37 patients. For each patient, we performed a pixel-by-pixel analysis with a single irregularly shaped ROI encompassing all of the tumor in each plane, as identified from corresponding CT scans, and we analyzed all planes that included tumor in each study. The unit of analysis for these studies, thus, is each individual pixel. The software available to us previously (22) had limited analysis to small rectangular-shaped adjacent ROIs drawn over the tumor, making the unit of analysis an ROI averaging about 25 pixels and introducing the possibility of investigator bias in drawing ROIs. Additionally, only one representative central plane from each imaging study was analyzed in that earlier study. Tables 2–5 list the patients studied, grouped according to type of tumor. The tumor stage, form of radiotherapy the patient received, and pretreatment FHV are included, as well as the median and range of FHVs for the different tumor groupings. For the largest subset of patients, those with nonsmall cell lung cancer ($n = 21$; Table

Table 2. Nonsmall cell lung cancer patients with pretreatment FMISO scans

Patient code	Tumor type and stage (TNM)	Type of scan	Type of treatment	Pretreatment FHV, %
6	Nonsmall cell lung CA T3N1	Cont	Neutrons	29.4
11	Nonsmall cell lung CA T3N3M1, L neck node	Int	Photons	3.0
12	Nonsmall cell lung CA T3N1M0	Int	Photons	20.7
14	Nonsmall cell lung CA T4N0M1	Int	Neutrons	90.7
22	Nonsmall cell lung CA T2N3M0	Int	Neutrons	47.6
25*	Nonsmall cell lung CA T1N3M0	Brief	Neutrons	19.7
26*	Nonsmall cell lung CA T3N0M0	Brief	Neutrons	70.6
27	Nonsmall cell lung CA T4N2M0	Brief	Neutrons	53.9
28*	Nonsmall cell lung CA T2N3M0	Brief	Photons	58.3
29	Nonsmall cell lung CA T3N2M0	Brief	Photons	36.1
30	Nonsmall cell lung CA TxN3M1	Brief	Neutrons	37.7
31*	Nonsmall cell lung CA T3N2M0	Brief	Neutrons	51.4
32	Nonsmall cell lung CA T4N2M0	Int	Neutrons	1.3
33*	Nonsmall cell lung CA T3N2M0	Int	Neutrons	32.1
34*	Nonsmall cell lung CA T4N0M0	Int	Photons	78.4
35	Nonsmall cell lung CA T2N2M0	Int	Photons and chemo	24.6
36	Nonsmall cell lung CA T3N2M0	Int	Neutrons	75.4
37	Nonsmall cell lung CA T4N3M0	Int	Never received treatment	94.7
38	Nonsmall cell lung CA T4N3M1	Int	Photons	77.4
40*	Nonsmall cell lung CA T4N1M0	Int	Photons and chemo	83.8
43	Nonsmall cell lung CA T3N2M0	Int	Neutrons	5.9
				Median = 47.6
				Range = 1.3–94.7

FMISO = fluoromisonidazole.

FHV = fractional hypoxic volume.

CA = cancer.

PET = positron emission tomography.

* Pretreatment fractional hypoxic volumes for these 7 patients were also reported in another article on changes in tumor oxygenation during radiotherapy, as assessed by repeated FMISO scans. (21) They are included here for completeness. In Koh *et al.*, (21), FHV was based on those PET image planes common to the initial scan and the one to three follow-up scans. Thus, not all planes were necessarily analyzed in the first scan in that series, and so FHV's for some of those patients differ from the FHV's reported here.

2), the median FHV was 47.6%, with a range of 1.3% to 94.7%. For the seven head and neck cancers (Table 3), the median FHV was markedly lower at 8.81%, with a range of 0.2 to 18.9%. The four prostate tumors had a wide range of FHV's, from 0 to 93.9% (Table 4), and in the mixed group of tumors including one each of renal cell, thyroid, breast, cervix, and rectal carcinomas, the median FHV was 55.2% and the range, 21.4 to 85.8% (Table 5). The cumulative percentages of FHV's for nonsmall cell lung and head and neck carcinomas (Fig. 2) demonstrate the markedly higher FHV's seen in the lung tumors, which also tended to be much larger than most of the tumors in the other sites.

The FHV reported for each patient in Tables 2–5 is summed over all image planes containing tumor identifiable in the matched CT scans. In 24 of 37 patients (64.9%), tumor was included in three or four planes, thus allowing some estimate of heterogeneity in distribution of hypoxic regions within a single tumor. Hypoxia was distributed very heterogeneously across many tumors. For example, in 15 of 24 patients (62.5%) with tumor in multiple planes, the most hypoxic plane had a FHV at least twice as great as that of the least hypoxic plane. In 9 of 24 patients (37.5%), the FHV of the most and least hy-

poxic planes differed by a factor of 10 or more. In 7 of 24 patients (29.2%), at least one plane showed no significant hypoxia (no pixels with an FMISO tumor:blood ratio ≥ 1.4). This heterogeneous hypoxia distribution is well illustrated by a nonsmall cell lung carcinoma in patient 33 (Fig. 3). This large tumor (156 cc) was visible in four consecutive imaging planes with FHV's of 0%, 50.6%, 35.5%, and 34.6%, respectively. The distribution of hypoxic regions within each image plane does not suggest a pattern of central hypoxia.

We were able to measure the volume of 12 nonsmall cell lung cancers from the patients' CT scans. When the tumor size in cc was compared to the FHV (Fig. 4), there was no significant correlation ($r^2 = 0.035$).

DISCUSSION

Earlier studies from our research group have emphasized quantitative validation of [¹⁸F]FMISO as an imaging agent for tumor hypoxia. Initial studies characterized the binding of FMISO labeled with ³H or ¹⁸F in rodent tumors and cell cultures *in vitro* (34, 36). Imaging protocols were then developed in dogs with spontaneous tumors (35) and refined for use in our first human studies (22). In a recent

Table 3. Head and neck cancer patients with pretreatment FMISO images

Patient code	Tumor type and stage	Type of scan	Type of treatment	Pretreatment FHV, %
2	Tongue adenoid cystic CA T4N1M0	Cont	Neutrons	15.5
3	Oral tongue squamous cell CA T4N3M0	Int	Neutrons	8.8
4	Infratemporal adenoid cystic CA — recurrent T3N0M0	Cont	Neutrons	12.8
7	Parotid adenoCA T4N2b	Cont	Neutrons	18.9
9	Tonsillar fossa squamous cell CA T4N3M0	Int	Neutrons	5.5
10	Tongue squamous CA T4N2M0	Int	Neutrons	0.2
18	Recurrent max sinus adenoid cystic CA T3N0M0	Int	Neutrons	1.2
				Median = 8.8
				Range = 0.2–18.9

FMISO = fluoromisonidazole.

FHV = fractional hypoxic volume.

CA = cancer.

report on changes in tumor oxygenation during therapy (21) and in the studies presented here, we have refined our image analysis to make it more quantitative and to assess regional hypoxia within each tumor.

Our [^{18}F]FMISO imaging data were analyzed pixel-by-pixel to encompass all of the tumor volume in each plane, as defined by CT scans. This analysis revealed measurable hypoxia in nearly all the 37 imaged tumors of various sizes and histologies. Only 5 of 37 tumors (13.5%) had FHV \leq 5%, including one who had no measurable hypoxia (0% FHV). In our initial report (22), we observed that two of eight tumors (25%) failed to show significant hypoxia. The sample size was small and the analysis less complete; only one representative plane was analyzed from each tumor and the image analysis software precluded drawing irregular ROIs around the whole tumor and doing pixel-by-pixel analysis of tumor:blood ratios, as reported here. No other imaging study has presented pixel-by-pixel analysis, and those studies also report a lower incidence and extent of hypoxia than we have observed in the current series. Valk *et al.* (43) imaged two gliomas and one anaplastic astrocytoma after administration of [^{18}F]FMISO. Two of the three tumors showed increased uptake of FMISO at 2–3 h postinjection, with tumor:plasma ratios of 1.10 and 1.49 for the whole tumor. For one of the gliomas, the whole tumor:plasma ratio was less than 1.0.

Single photon emission computed tomography imaging studies of tumors with [^{123}I]IAZA, another radiolabeled nitroimidazole, have been reported (13, 31). Parliament *et al.* (31) defined ROIs to examine focal accumulation of [^{123}I]IAZA in SPECT images of tumors taken 16 to 24 h after injection of tracer. They reported that 3 of 10 tumors (a malignant fibrous histiocytoma, a primary small cell lung cancer, and small cell lung cancer metastatic to brain) were IAZA-avid: scans done 16–24 h. after tracer injection produced tumor:normal tissue ratios that were increased by 16 to 39%, relative to scans done shortly after IAZA administration. The other 7 of 10 tumors had tumor to normal tissue ratios that were –10% to +9% different from the early images and were interpreted as not having significant binding. Groshar *et al.* (13) reported the results of SPECT imaging of [^{123}I]IAZA in 27 tumors of varying histologies in 22 patients. In this series, 13 of 27 tumors (48.1%) showed increased uptake relative to contralateral normal tissue, 13 of 27 (48.1%) showed equal uptake, and 1 tumor showed decreased uptake. Thus, approximately one-third to one-half of the tumors appeared to be hypoxic when imaged with [^{123}I]IAZA at 16 to 24 h after tracer administration, much less than the 75 to 97% studied with [^{18}F]FMISO at 2 to 3 h after injection in our two reports. Several factors may contribute to these differences. The imaging protocols, methods of analysis, and the tracers

Table 4. Prostate cancer patients with pretreatment FMISO scans

Patient code	Tumor type and stage	Type of scan	Type of treatment	Pretreatment FHV, %
8	Prostate adenoCA T3N0M1	Int	Neutrons	93.9
13	Prostate adenoCA T2aN0M0	Int	Photons	20.7
			Neutron boost	
15	Prostate adenoCA T3N0M0	Int	Neutrons	0
17	Prostate adenoCA T2bN0M0	Int	Neutrons	15.7
				Median = 18.2
				Range = 0–93.9

Table 5. Miscellaneous patients with pretreatment FMISO scans

Patient code	Tumor type and stage	Type of scan	Type of treatment	Pretreatment FHV, %
5	Renal cell CA TxNxM1	Int	Photons	55.2
16	Metastatic breast adenoCA TxNxM1	Int	Photons	21.4
9	Recurrent rectal adenoCA T4N0M0	Int	Neutrons	69.1
21	Medullary CA Thyroid T4NxM1	Int	Neutrons	24.0
39	Cervical squamous cell CA T3bN1M0	Int	Neutrons (1 fx), photons	85.8
				Median = 55.2
				Range = 21.4–85.8

FMISO = fluoromisonidazole.

FHV = fractional hypoxic volume.

CA = cancer.

differ between the studies, and a wide variety of tumor types have been examined. Techniques that use a global averaging method could well miss focal but biologically significant areas of hypoxia. It, thus, is not possible to make direct comparison between the global tumor to normal tissue ratios and the pixel-by-pixel analysis reported here, wherein small regions of hypoxia may be detected. In addition, differences between the two tracers should be considered. [¹²³I]IAZA deiodinates *in vivo*, as indicated by substantial uptake into thyroid (28). [¹⁸F]FMISO is highly stable after injection. No FMISO metabolites were found in blood of mice or humans up to 2 h after drug administration (3, 36). Uptake of ¹⁸F into bone would indicate free fluorine; this has never been seen.

In vitro studies show that very low oxygen levels are required for substantial uptake of FMISO by cells. The oxygen level inhibiting FMISO binding by 50%, relative to binding under anoxic conditions, varied from 720 to

2300 ppm (0.55 to 1.75 mmHg) in four cell lines (36). This implies that some regions with oxygen levels at or below 1–2 mmHg exist in the vast majority of tumors we have studied. It, thus, is interesting to compare the high proportion of tumors showing hypoxia with FMISO imaging to studies with O₂ electrodes in human tumors.

Recent studies with oxygen electrodes, principally the Eppendorf pO₂ histogram, have quantified oxygen distributions in metastases from squamous cell carcinomas of the head and neck (9, 24), carcinomas of the breast and cervix (16–18, 45), and primary gliomas as well as less aggressive primary brain tumors (33), metastatic brain tumors (33), and soft tissue sarcomas (2). Results of these studies are summarized in Table 6. In some types of malignancies, specifically carcinomas of breast and cervix, a substantial fraction of the tumors showed no pO₂ values below 2.5 or 5 mmHg. The data from cervical cancer are interesting, as tumors in this site historically have been considered those in which hypoxia occurs and possibly limits response to radiotherapy. These electrode data demonstrate marked patient-to-patient variability and point out the critical importance of measures in individual patients; generalizations based on tumor size or stage are not possible (16–18, 23). In contrast to breast and cervical carcinomas, 73% of neck node metastases from head and neck tumors and 80–100% of primary brain tumors, brain metastases, and soft tissue sarcomas have a measurable ‘hypoxic fraction’; that is, some tumor regions residing at a pO₂ below a cutoff value of 2 to 5 mmHg (2, 24, 33). It is clear that the frequency of the very low O₂ levels necessary for FMISO binding varies markedly between tumor types.

Most of the tumors imaged in our series are histologically different from those subjected to electrode measures and specific direct correlations cannot be made in the measurements made with the two assays. Factors in addition to low oxygen levels, such as oxygen-independent nitroreductase enzymes or thiol levels, may also influence nitroimidazole binding (5, 32). Until tumor enzyme or thiol levels are measured directly, it is not possible to determine the role of these complicating factors. Nonetheless, some

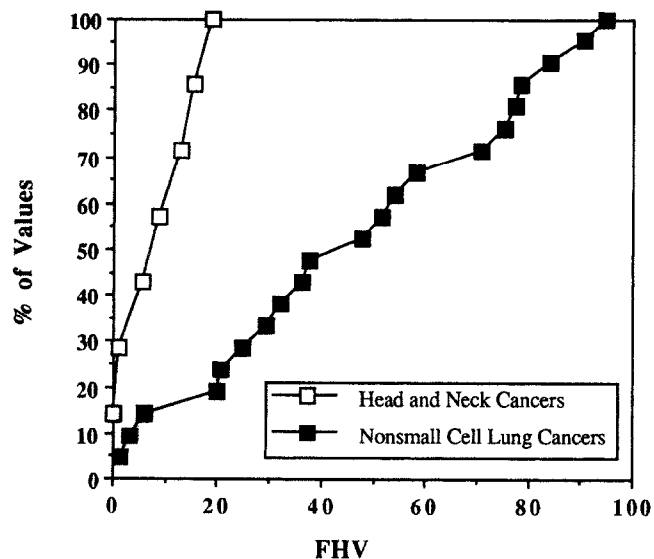
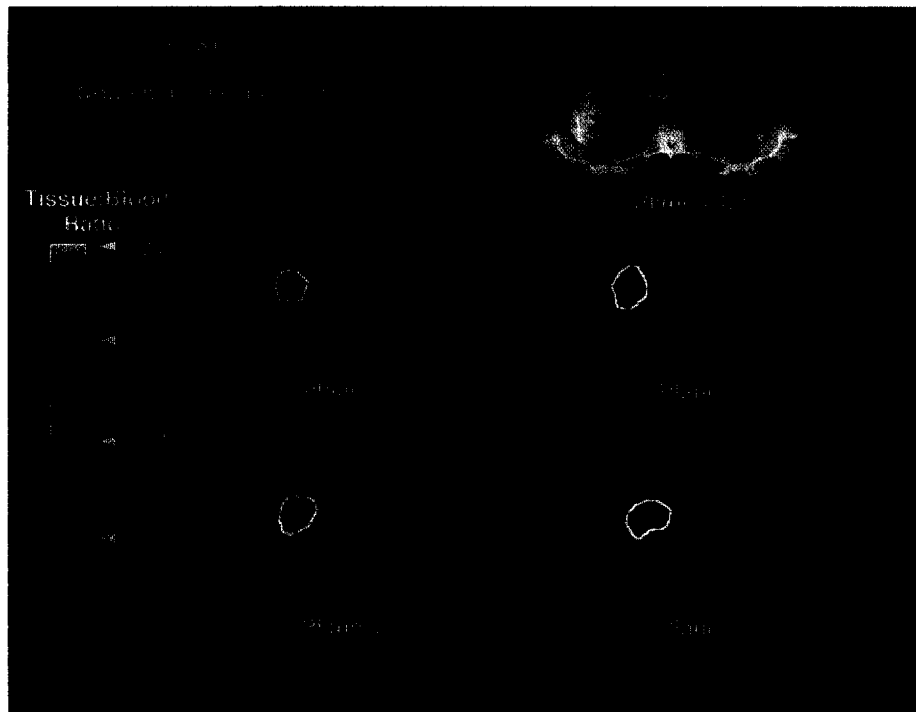
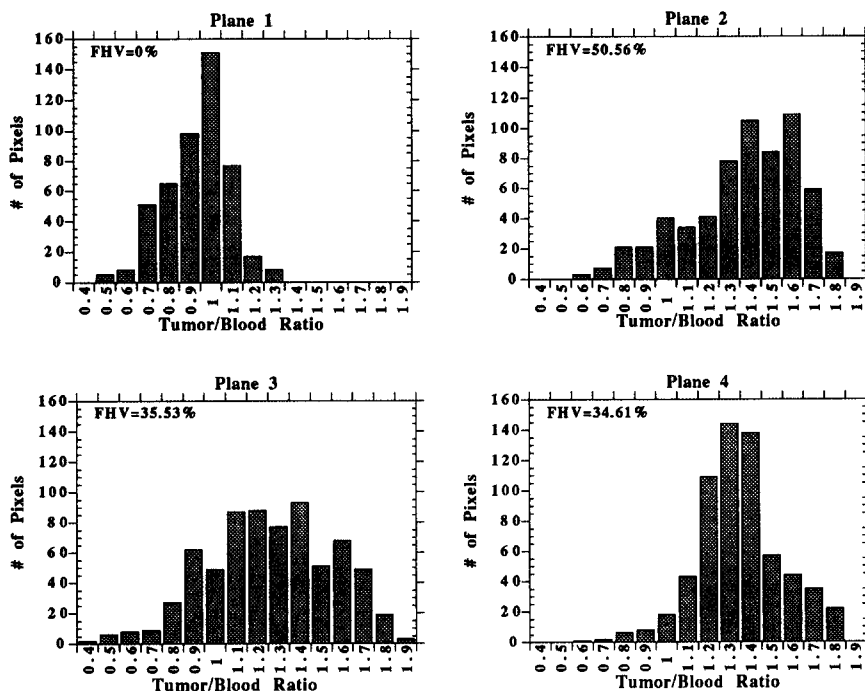


Fig. 2. Cumulative percent of patients with head and neck carcinomas ($n = 7$) and nonsmall cell lung carcinomas ($n = 21$) as a function of fractional hypoxic volume.



(a)



(b)

Fig. 3. (a) The heterogeneity of hypoxia between different regions within one tumor is shown in images of a nonsmall cell lung cancer, study 33. Tumor was present in four contiguous planes. The fractional hypoxic volumes were 0%, 50.6%, 35.5%, and 34.6%, for planes 1, 2, 3, and 4, respectively. The total fractional hypoxic volume for this tumor was 32.1%. (b) Histograms of the distribution of pixels at different tumor: blood ratios in each of the four image planes in Fig. 3(a).

broad comparisons can be made between the electrode data of Gatenby *et al.* (9) and Lartigau *et al.* (24) for head and neck tumors and our imaging studies. All seven primary head and neck cancers imaged in our series showed

evidence of hypoxia, with the least hypoxic tumor having a FHV of 0.2%. That low level of hypoxia likely would have been missed if we had not imaged and analyzed the whole tumor. The inability to sample the whole tumor may

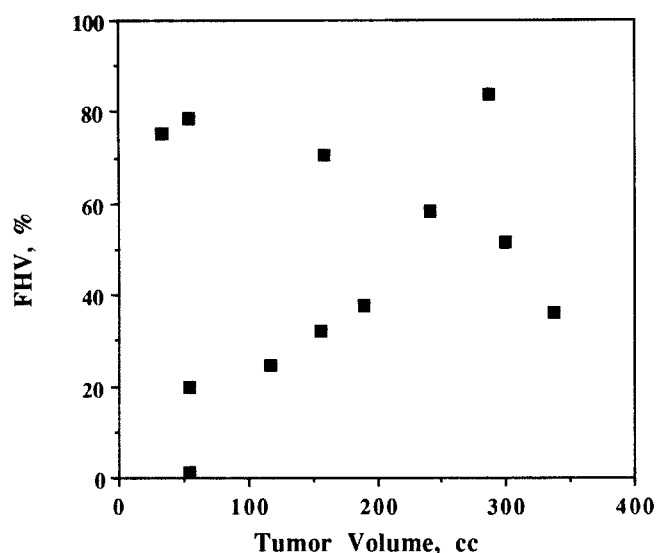


Fig. 4. Fractional hypoxic volume vs. tumor size for 12 nonsmall cell lung cancers, for which tumor volumes could be measured from the computed tomography scans.

be one factor explaining why other investigators have reported a lower proportion of head and neck cancers with demonstrable hypoxia. Gatenby reported that 81% of the metastatic neck nodes in his study had some or all of their O_2 measures below 10 mmHg. Lartigau *et al.* (24) also measured pO_2 in neck node metastases from head and neck primary tumors and reported that 9 of 15 tumors (73.3%) had some values below 2.0 mmHg (Table 6). Imaging of the whole tumor accompanied by analysis on a pixel-by-pixel basis may be more sensitive and identify

foci of hypoxia that are missed by limited sampling from electrodes or by imaging studies that calculate a global tumor:plasma or tumor:normal tissue ratio. This may be one of the strongest points of PET. Even considering that our images of primary tumors may not represent the physiology of lymph node metastases, the O_2 electrode and FMISO data in head and neck cancers are consistent with each other. Direct comparisons of both methods in the same tumors would clarify the above results.

Measurements with electrodes and FMISO images both suggest that hypoxia is present in a large proportion of some types of tumors, while electrode measurements suggest that tumors in other sites are less likely to have measurable hypoxia and/or have, on average, much smaller hypoxic fractions. In most primary and metastatic brain tumors and soft tissue sarcomas, the proportion of tumors with low O_2 levels (89–95%) is comparable to the 89% of tumors in our series that had a FHV $\geq 5\%$. However, it should be emphasized that the relation between FHV and the proportion of tumor electrode measures below 2.5 or 5 mmHg is not yet defined, and it is premature to speculate further on the significance of these similarities. Direct comparisons of FMISO imaging and O_2 electrodes in the same tumors will answer this question.

Both electrode measurements and our FMISO images demonstrate heterogeneity of hypoxia between individual tumors of similar histology and site. In nonsmall cell lung cancers, the FHV varies from 1.3 to 94.7% and in the seven head and neck cancers, FHVs range from 0.2 to 18.8%. Hypoxic fractions in tumors sampled with electrodes, defined as the proportion of measurements below

Table 6. Tumor hypoxic fractions measured with oxygen electrodes

Tumor type (number of patients)	Hypoxia criterion	Percent of tumors with hypoxia*	Hypoxic fraction in subset of tumors showing hypoxia.† mean (range)	Reference
Neck node metastases, head and neck				
CA primaries (15)	< 2.0 mmHg	73.3%‡	28.6% (3–100%)	24
Breast CA (15)	< 2.5 mmHg	33%	17.4% (3–49%)	45
Glioblastoma (10)	< 2.5 mmHg	100%	42.1% (9.5–68.5%)	33
Misc primary brain tumors (5)	< 2.5 mmHg	80%	23.1% (9.0–41.5%)	33
Brain metastases, various primaries (5)	< 2.5 mmHg	100%	26.0% (1.5–46.5%)	33
Cervical CA (18)	< 2.5 mmHg	27.8%	6.0% (1–13%)	17
Cervical CA (31)	< 5 mmHg	67.7%	NA§ (2–96%)	16
Cervical CA (50)	< 5 mmHg	50.0%	NA	18
Soft tissue sarcomas (9)	< 5 mmHg	88.8%	32.6% (9–76%)	2
Neck node metastases, head and neck				
CA primaries (31)	< 10 mmHg	80.6%	NA	9

CA = cancer.

* Tumors with hypoxia were those that had any pO_2 measurements below the cutoff value.

† Hypoxic fraction is defined as the % of pO_2 measures at or below the cutoff for hypoxia. Tumors with hypoxic fractions of zero were not included in this average.

‡ In 6 of 15 patients, O_2 recordings were made along two tracks and the authors reported two different values for % of measures below 2.0 mmHg. A tumor was considered hypoxic if there were some measures below 2.0 mm in either track.

§ NA = information not available.

|| Averaged from histographic hypoxic fractions, Table 3, Brizel *et al.* 1994.

2.5 or 5 mmHg, ranged from 0 to 76% in sarcomas [5 mmHg upper limit; (2)], from 9.5 to 68.5% in gliomas [2.5 mmHg upper limit; (33)], and 0–96% in cervical cancer [5 mmHg upper limit; (16)]. Comparison of pO₂ histograms for individual breast or cervical carcinomas of the same stage (17, 45) or for sarcomas (2) also supports tumor to tumor heterogeneity.

Our FMISO images also show marked variation of hypoxic regions within one tumor [Fig. 3; (21)]. There is no strong evidence of hypoxia being centrally located in tumors imaged with FMISO, or indeed, evidence for any single pattern. This observation is consistent with patterns of binding of [¹⁴C]MISO in rodent tumors (4) where areas of heavy labeling were not obviously associated with regions of necrosis or distance from blood vessels. Regional mapping of tumors done with electrodes under CT guidance also suggests intratumor variability (2). Brizel *et al.* (2) mapped pO₂ at 0.7 mm intervals along several tracks in each of nine soft tissue sarcomas. They observed no predictable correlation between pO₂ and depth of electrode in the tumor and also reported major variation in oxygen levels along each track and between tracks within one tumor. In contrast, Gatenby *et al.* (8) measured oxygen levels in several tumor types, including squamous cell carcinomas of the head and neck, colon adenocarcinomas, and lung tumors and reported that central hypoxia was the most prevalent pattern, occurring in nine of 15 tumors. The remaining tumors were reported to have uniform oxygen distribution, except for one with a lateral-to-medial gradient. Approximately 20 measures were made per tumor, and thus variations of oxygenation over small regions may have been missed.

In transplanted rodent tumors, radiobiologic hypoxic fraction assessed from the radiation response of the neoplasms, and extent of hypoxia measured with electrodes both increase with increasing tumor size (29, 44). The data from human tumors are less consistent. Vaupel *et al.* (45) and Hockel *et al.* (17) reported no correlation between stage of breast or cervical cancer and proportion of pO₂ values below 2.5 or 5 mmHg. In our studies with FMISO imaging of lung tumors [Fig. 4; (21)] and in Gatenby's (9) electrode measurements in neck node metastases from head and neck cancers, tumor volume was measured and compared directly to extent of hypoxia. There was no correlation between the two parameters. However, Brizel *et al.* (2) reported a positive correlation of hypoxic fractions with size in sarcomas, and Lartigau *et al.* (24) reported a significantly lower mean pO₂ in N3 neck nodes (mean: 17 mmHg) than in N2 nodes (mean: 25 mm).

When human tumors are big enough to be detected, they already are large in comparison to many rodent tumors, which rarely exceed a few grams. Thus, it is not surprising that the tumor volume-hypoxic fraction correlation does not always hold in human neoplasms. Certainly, the non-small cell lung tumors analyzed for Fig. 4 were very large, with volumes ranging from 34 to 300 cc; 8 of the 12 patients had tumors of greater than 100 cc. Intertumor and intratumor comparisons of hypoxia detected with O₂ electrodes or FMISO imaging suggest that patterns of tumor hypoxia vary markedly between and within tumor type and are only sometimes positively correlated with tumor stage or size.

The initial rationale for determining extent of tumor hypoxia prior to radiotherapy was to determine if low oxygen levels predict poorer local control. Two factors precluded any meaningful measurement of this endpoint in our FMISO imaging studies. First, of the 37 patients imaged in this series, 24 (65%) received neutron treatment only, and 2 patients received both neutrons and photons. Hypoxia is expected to have less effect on the outcome of neutron therapy than is the case for photons. Second, the non-small cell lung cancer patients, the largest group in our series, typically succumb to metastatic disease and provide poor follow-up for assessment of local control of the irradiated primary tumor. Fluoromisonidazole imaging ideally would be evaluated in patients undergoing primary photon therapy alone for loco-regional control of tumor, or alternately, patients designated to receive a hypoxic cell cytotoxin, such as mitomycin C or tirapazamine. The current standard of cancer treatment at the University of Washington Medical Center, and in many other cancer centers, dictates that relatively few patients are treated with photon radiotherapy alone. Surgery and/or chemotherapy are often added in the multimodal management of local regionally advanced tumors. It is appropriate that cancer patients receive more aggressive treatment when it improves their chance of local control or cure. However, it is increasingly difficult to get a direct answer to the question we originally posed when we began hypoxia imaging: what is the role of hypoxia in a tumor's response to conventional primary radiotherapy? The utility of hypoxia imaging in cancer therapy will have to be determined in the environment of multimodality treatment. A large body of data suggest hypoxia influences tumor response to conventional chemotherapy as well as to drugs tailored to kill oxygen-deprived cells. Hypoxia also may enhance malignant progression. For these reasons we believe it remains important to assess tumor hypoxia in many different tumor types and in individual patients.

REFERENCES

1. Anderson, G. R.; Stoler, D. L.; Scarcello, L. A. Normal fibroblasts responding to anoxia exhibit features of the malignant phenotype. *J. Biol. Chem.* 264(25):14885–14892; 1989.
2. Brizel, D. M.; Rosner, G. L.; Harrelson, J.; Prosnitz, L. R.; Dewhirst, M. W. Pretreatment oxygenation profiles of human soft tissue sarcomas. *Int. J. Radiat. Oncol. Biol. Phys.* 30(3):635–642; 1994.

3. Casciari, J. J.; Graham, M. M.; Rasey, J. S. A modeling approach for quantifying tumor hypoxia with [F-18]fluoromisonidazole PET time-activity data. *Med. Phys.* 22(7):1127–1139; 1995.
4. Chapman, J. D. The detection and measurement of hypoxic cells in solid tumors. *Cancer* 54:2441–2449; 1984.
5. Cobb, L. M.; Nolan, J.; Butler, S. Tissue distribution of ¹⁴C- and ³H-labelled misonidazole in the tumor-bearing mouse. *Int. J. Radiat. Oncol. Biol. Phys.* 18:347–351; 1989.
6. Coleman, C. N. Hypoxia in tumors: A paradigm for the approach to biochemical and physiological heterogeneity. *J. Natl. Cancer Inst.* 80:310–317; 1988.
7. Fenton, B. M.; Rofstad, E. K.; Degner, F. L.; Sutherland, R. M. Cryospectrophotometric determination of tumor intravascular oxyhemoglobin saturations: Dependence on vascular geometry and tumor growth. *J. Natl. Cancer Inst.* 80(20):1612–1619; 1988.
8. Gatenby, R. A.; Coia, L. R.; Richter, M. P.; Katz, H.; Moldofsky, P. J.; Engstrom, P.; Brown, D. Q.; Brookland, R.; Broder, G. J. Oxygen tension in human tumors: *In vivo* mapping using CT-guided probes. *Radiology* 156:211–214; 1985.
9. Gatenby, R. A.; Kessler, H. B.; Rosenblum, J. S.; Coia, L. R.; Moldofsky, P. J.; Hartz, W. H.; Broder, G. J. Oxygen distribution in squamous cell carcinoma metastases and its relationship to outcome of radiation therapy. *Int. J. Radiat. Oncol. Biol. Phys.* 14(5):831–838; 1988.
10. Graeber, T. G.; Osmanian, C.; Jacks, T.; Housman, D. E.; Kochs, C. J.; Lowe, S. W.; Giaccia, A. J. Hypoxia-mediated selection of cells with diminished apoptotic potential in solid tumours. *Nature* 379:88–91; 1996.
11. Graham, M. M. and Lewellen, B. L. High speed automated discrete blood sampling for positron emission tomography. *J. Nucl. Med.* 34(1):357–1360; 1993.
12. Grierson, J. R.; Link, J. M.; Mathis, C. A.; Rasey, J. S.; Krohn, K. A. A radiosynthesis of fluorine-18 fluoromisonidazole. *J. Nucl. Med.* 30:343–350; 1989.
13. Groshar, D.; McEwan, A. J. B.; Parliament, M. B.; Urtasun, R. C.; Golberg, L. E.; Hoskinson, M.; Mercer, J. R.; Mannan, R. H.; Wiebe, L. I.; Chapman, J. D. Imaging tumor hypoxia and tumor perfusion. *J. Nucl. Med.* 34(6):885–888; 1993.
14. Hill, R. P. Tumor progression: Potential role of unstable genomic changes. *Cancer Metastasis Rev.* 9(2):137–147; 1990.
15. Hlatky, L.; Tsionou, C.; Hahnfeldt, P.; Coleman, C. N. Mammary fibroblasts may influence breast tumor angiogenesis, via hypoxia-induced vascular endothelial growth factor upregulation and protein expression. *Cancer Res.* 54(23):6083–6086; 1994.
16. Höckel, M.; Knoop, C.; Schlenger, K.; Vorndran, B.; Baußmann, E.; Mitze, M.; Knapstein, P. G.; Vaupel, P. Intratumoral pO₂ predicts survival in advanced cancer of the uterine cervix. *Radiother. Oncol.* 26:45–50; 1993.
17. Höckel, M.; Schlenger, K.; Knoop, C.; Vaupel, P. Oxygenation of carcinomas of the uterine cervix: Evaluation by computerized O₂ tension measurements. *Cancer Res.* 51:6098–6102; 1991.
18. Höckel, M.; Vorndran, B.; Schlenger, K.; Baußmann, E.; Knapstein, P. G. Tumor oxygenation: A new predictive parameter in locally advanced cancer of the uterine cervix. *Gynecol. Oncol.* 51:141–149; 1993.
19. Kallinowski, F.; Zander, R.; Hoeckel, M.; Vaupel, P. Tumor tissue oxygenation as evaluated by computerized-pO₂-histography. *Int. J. Radiat. Oncol. Biol. Phys.* 19:953–961; 1990.
20. Kalra, R.; Jones, A.-M.; Kirk, J.; Adams, G. E.; Stratford, I. J. The effect of hypoxia on acquired drug resistance and response to epidermal growth factor in Chinese hamster lung fibroblasts and human breast-cancer cells *in vitro*. *Int. J. Cancer* 54:650–655; 1993.
21. Koh, W.-J.; Bergman, K. S.; Rasey, J. S.; Peterson, L. M.; Evans, M. L.; Graham, M. M.; Grierson, J. R.; Lewellen, T. K.; Krohn, K. A.; Griffin, T. W. Evaluation of oxygenation status during fractionated radiotherapy in human nonsmall cell lung cancers using [F-18]fluoromisonidazole positron emission tomography. *Int. J. Radiat. Oncol. Biol. Phys.* 33(2):391–398; 1995.
22. Koh, W.-J.; Rasey, J. S.; Evans, M. L.; Grierson, J. R.; Lewellen, T. K.; Graham, M. M.; Krohn, K. A.; Griffin, T. W. Imaging of hypoxia in human tumors with [F-18]fluoromisonidazole. *Int. J. Radiat. Oncol. Biol. Phys.* 22:1–13; 1992.
23. Kolstad, P. Intercapillary distance, oxygen tension and local recurrence in cervix cancer. *Scand. J. Clin. Lab. Invest. Suppl.* 106:145–157; 1968.
24. Lartigau, E.; Le Ridant, A.-M.; Lambin, P.; Weeger, P.; Martin, L.; Sigal, R.; Lusinchi, A.; Luboinski, B.; Eschwege, F.; Guichard, M. Oxygenation of head and neck tumors. *Cancer* 71(7):2319–2325; 1993.
25. Lewellen, T. K.; Bice, A. N.; Harrison, R. L.; Pencke, M. D.; Link, J. M. Performance measurements of the SP-3000/UW time of flight emission tomograph. *IEEE Trans. Nucl. Sci.* 35(1):665–667; 1988.
26. Lewellen, T. K.; Miyaoka, R. S.; Kohlmyer, S. G. Improving the performance of the SP-3000 PET detector modules. *IEEE Trans. Nucl. Sci.* 39(1):364–1368; 1992.
27. Luk, C. K.; Veinot-Drebot, L.; Tjan, E.; Tannock, I. F. Effect of transient hypoxia on sensitivity to doxorubicin in human and murine cell lines. *J. Natl. Cancer Inst.* 82:684–692; 1990.
28. Mannan, R. H.; Somayaji, V. V.; Lee, J.; Mercer, J. R.; Chapman, D.; Wiebe, L. I. Radioiodinated 1-(5-Iodo-5-deoxy-β-D-arabinofuranosyl)-2-nitroimidazole (Iodoazomycin Arabinoside: IAZA): A novel marker of tissue hypoxia. *J. Nucl. Med.* 32(9):1764–1770; 1991.
29. Moulder, J. E.; Rockwell, S. Tumor hypoxia: Its impact on cancer therapy. *Cancer Metastasis Rev.* 5:313–341; 1987.
30. Olive, P. L.; Durand, R. E. Detection of hypoxic cells in a murine tumor with the use of the comet assay. *J. Natl. Cancer Inst.* 84:707–711; 1992.
31. Parliament, M. B.; Chapman, J. D.; Urtasun, R. C.; McEwan, A. J.; Golberg, L.; Mercer, J. R.; Mannan, R. H.; Wiebe, L. I. Noninvasive assessment of human tumour hypoxia with 123 I-iodoazomycin arabinoside: Preliminary report of a clinical study. *Br. J. Cancer* 65:90–95; 1992.
32. Raleigh, J. A.; Koch, C. J. The importance of thiols in the reductive binding of 2-nitroimidazoles to macromolecules. *Biochem. Pharmacol.* 40:2457–2464; 1990.
33. Rampling, R.; Cruickshank, G.; Lewis, A. D.; Fitzsimmons, S. A.; Workman, P. Direct measurement of pO₂ distribution and bioreductive enzymes in human malignant brain tumors. *Int. J. Radiat. Oncol. Biol. Phys.* 29(3):427–431; 1994.
34. Rasey, J. S.; Grunbaum, Z.; Magee, S.; Nelson, N. J.; Olive, P. L.; Durand, R. E.; Krohn, K. A. Characterization of radiolabeled fluoromisonidazole as a probe for hypoxic cells. *Radiat. Res.* 111:292–304; 1987.
35. Rasey, J. S.; Koh, W.-J.; Grierson, J. R.; Grunbaum, Z.; Krohn, K. A. Radiolabeled fluoromisonidazole as an imaging agent for tumor hypoxia. *Int. J. Radiat. Oncol. Biol. Phys.* 17:985–991; 1989.
36. Rasey, J. S.; Nelson, N. J.; Chin, L.; Evans, M. L.; Grunbaum, Z. Characteristics of the binding of labeled fluoromisonidazole in cells *in vitro*. *Radiat. Res.* 122:301–308; 1990.
37. Rice, G. C.; Hoy, C.; Schimke, R. T. Transient hypoxia enhances the frequency of dihydrofolate reductase gene amplification in Chinese hamster ovary cells. *Proc. Natl. Acad. Sci. USA* 83:5978–5982; 1986.
38. Rice, G. C.; Ling, V.; Schimke, R. T. Frequencies of independent and simultaneous selection of Chinese hamster cells for methotrexate and doxorubicin (adriamycin) resistance. *Proc. Natl. Acad. Sci. USA* 84:9261–9264; 1987.

39. Rockwell, S. Effect of some proliferative and environmental factors on the toxicity of mitomycin C to tumor cells *in vitro*. *Int. J. Cancer* 38:229–235; 1986.
40. Rockwell, S.; Keyes, S. R.; Sartorelli, A. C. Preclinical studies of porfiromycin as an adjunct to radiotherapy. *Radiat. Res.* 116:100–113; 1988.
41. Sakata, K.; Kwok, T. T.; Murphy, B. J.; Laderoute, K. R.; Gordon, G. R.; Sutherland, R. M. Hypoxia-induced drug resistance: Comparison to P-glycoprotein-associated drug resistance. *Br. J. Cancer* 64:809–814; 1991.
42. Teicher, B. A.; Lazo, J. S.; Sartorelli, A. C. Classification of antineoplastic agents by their selective toxicities toward oxygenated and hypoxic tumor cells. *Cancer Res.* 41(1):73–81; 1981.
43. Valk, P. E.; Mathis, C. A.; Prados, M. D.; Gilbert, J. C.; Budinger, T. F. Hypoxia in human gliomas: Demonstration by PET with fluorine-18-fluoromisonidazole. *J. Nucl. Med.* 33(12):2133–2137; 1992.
44. Vaupel, P.; Okunieff, P.; Kallinowski, F.; Neuringer, L. J. Correlations between ³¹P-NMR spectroscopy and tissue O₂ tension measurements in a murine fibrosarcoma. *Radiat. Res.* 120:477–493; 1989.
45. Vaupel, P.; Schlenger, K.; Knoop, C.; Höckel, M. Oxygenation of human tumors: Evaluation of tissue oxygen distribution in breast cancers by computerized O₂ tension measurements. *Cancer Res.* 51:3316–3322; 1991.
46. Young, S. D.; Hill, R. P. Effects of reoxygenation on cells from hypoxic regions of solid tumors: Analysis of transplanted murine tumors for evidence of DNA overreplication. *Cancer Res.* 50:5031–5038; 1990.
47. Young, S. D.; Hill, R. P. Effects of reoxygenation on cells from hypoxic regions of solid tumors: Anticancer drug sensitivity and metastatic potential. *J. Natl. Cancer Inst.* 82(5):371–380; 1990.